Integrative Biology

Accepted Manuscript

ROYAL SOCIETY OF CHEMISTRY

www.rsc.org/ibiology

Pump-free multi-well-based microfluidic system for high-throughput analysis of size-control relative genes in budding yeast

Xianjie Kang[1, 2], Lingli Jiang[2], Xi Chen[2], Haiyu Yuan[1], Chunxiong Luo[1, 2],* Qi Ouyang[1, 2,3]*

[1]The State Key Laboratory for Artificial Microstructures and Mesoscopic Physics, School of Physics, Peking University, China, [2]Center for Quantitative Biology, Academy for Advanced Interdisciplinary Studies, Peking University, China. [3]Peking-Tsinghua Center for Life Sciences, Peking University, Beijing, 100871, China.

*To whom correspondence should be addressed: ChunxiongLuo, Email: pkuluocx@pku.edu.cn, Tel: +86-10-62754743; Qi Ouyang, Email: qi@pku.edu.cn, Tel: +86-10-62756943.

Abstract

Time-lapse single cell imaging through microscopy[1-2] can provide precise cell information such as cell size, cell cycle duration, protein localization and protein expression level et al. Usually, microfluidic system is needed in these measurements in order to provide a constant culture environment[3] and confine cells to grow in monolayer.[4-7] However, complex connection between channels inside chip and outside media, complex loading procedure of cells, withdraw its application in high-throughput single cell scanning experiments.[7-9] Here we provide a novel and easily operated pump-free multi-well-based microfluidic system which can high-throughput load many different budding yeast strains to monolayer growth conditions just by multi-channel pipette. Wild type budding yeast *(Saccharomyces cerevisiae)* and 62 different budding yeast size control relative gene deletion strains were chosen for scanning. We obtained the normalized statistical results of mother cell doubling time, daughter cell doubling time, mother cell size and daughter cell size of different gene deletion strains relative to the corresponding parameters of the wild type cells. Meanwhile, we compared typical cell morphology of different strains and analyzed the relationship between cell genotype and phenotype. This method which can be easily used in normal biology lab may help those researches who need to do high-throughput scanning of cell morphology and growth.

Keywords: high-throughput; pump-free microfluidic chip; single cell; budding yeast; cell size; doubling time.

1. Introduction

Cell phenotypes have been mainly investigated by population-wide methods that measure average behavior (cell size, grow rate, protein expression level) of cells in population level. For example, commonly used approaches for high-throughput, cell-based assays usually rely on a well-plate (96-, 384- and 1536-well) format.[10-12] This grow rate depended gene-relationship can be fast identified by the colony size. Despite the success of these assays, such population-wide studies mask the behavior of individual cells and are often insufficient for characterizing biological processes. For the measurement of cellular phenotype at single-cell level, flow cytometry[13] and automated microscopy[1-2] have been widely used. The high-throughput of flow cytometry combined with fluorescent labeling[14] has proved to be a very successful tool for single cell analysis. Although the high-throughput module can make flow cytometry analyze cell strains in high speed, it provides only a snapshot of single cell data at a series of single time points and cannot offer the ability to track a given single cell.

The limitations of methods mentioned above have been overcome after introducing microfluidic technologies,[15] in which microfluidic chip was combined with automated time-elapse live cell image acquisition. The microfluidic technologies can provide precise-controlled culture environment[3] and confine cells to grow several generations in monolayer[4-7] for better cell imaging. Tens of parallel experiments, such as different cell strains or culture environments, can be carried out on a single chip[7-9] to get more comparable data and save experiment time. But all the former setups require tens of tubes connection for each chip.[7-9] It wastes lots of time to prepare the connecting tubes, load cells for each channel and install the system which is also difficult to operate for a normal biologic experimenter.

The precise size control of cell is a basic biological function that influences nearly all aspects of cellular physiology. In budding yeast, it is regarded to be determined by the nutrition and cell grow rate in G1 phase.[16] It has attracted intensive research in molecular systems biology in the past few decades. For example, the pathways that couple cell grow and division in budding yeast were systematically identified by

Jorgensen in 2002.[17] Lots of abnormally small or large cells of gene deletion mutants were identified. Though more precise measurement can be achieved in their experiments, because the measurement of cell size by a Coulter Channelizer Z2 (Beckman-Coulter)[17-18] may introduce false information if some genes can influence the separation of mother and daughter, or the shape of the cell. It also cannot give precise measurement of cell cycle of daughter and mother cells.

In this paper, we present a simple but high-throughput multi-well microfluidic device. Just dropping 2μL solution of different cell types into the open wells of the chip by multi-pipette, cells will be loaded into microcavities through PDMS degassing and reabsorbing.[4] Cells of different sizes are restricted in chambers with the corresponding height where they grow in monolayer. This ensures that imaging of cells is in a single focal plane. We demonstrated the utility of the multi-well microfluidic chip with experimental data obtained from multiple budding yeast gene deletion mutants, which consist of the normalized statistical results of mother cell doubling time, daughter cell doubling time, mother cell size and daughter cell size of different gene deletion strains relative to the corresponding parameters of the wild type cells. Meanwhile, we compared typical cell morphology of some different strains and analyzed the relationship between cell genotype and phenotype. Besides precise measurement of cell size and doubling time, this chip can also serve for other research requiring long-term monitoring of single cell. It provides plenty of important advantages over existing approaches such as simplicity, integration, and high-throughput of measurement, representing an important contribution about taking quantitative single cell data to the field of systems biology.

2. Experimental section

2.1 Design and fabrication of multi-well microfluidic chip

The mold of our chip was constructed by patterning photoresist (SU-8, Clariant Corp.) on silicon wafer in a classical overlay lithography procedure. The chip was fabricated with PDMS (polydimethylsiloxane, RTV615, USA) using the standard soft lithographic technique (see supporting information). **Figure 1**a shows a schematic

image of our microfluidic chip (not to scale).The green part is the chip body made of PDMS; the blue part represents a 25 mm × 75 mm glass slide bonded with the chip body while the red part represents another 24 mm × 60 mm glass slide covering the chip body. The chip has 32 loading wells for different budding yeast samples. The figure pointed by the black dotted arrow shows the top-view of the structure of one of the 32 wells. The figure pointed by the black solid arrow is an enlarged three-dimensional architecture of the chambers linked to the well (not to scale), which consists of three parts: the first growth chamber has a height of about 7.1μm and a cross-sectional area of 180μm × 180μm (red); the second growth chamber has a height of about 4.2μm and a cross-sectional area of 180μm ×180μm (purple); the last enrichment chamber has a height of about 40μm and a cross-sectional area of 250μm ×500μm (green). The second growth chamber is connected to the first growth chamber through three fine necks which are 30μm wide and 4.2μm high (purple); and the last enrichment chamber is connected to the second growth chamber through three fine necks which are 30μm wide and about 2.0μm high (blue) (see **Figure 1**a). Here, different colors correspond to different height.

Figure 1b is the photo of the microfluidic chip under operation. In the experiments, different budding yeast strains were loaded into wells at the same time through multi-channel pipette. Tracking and timing observation for cell populations of 32 different budding yeast strains under same culture condition or different culture conditions can be realized with our multi-well microfluidic chip. **Figure 1**c schematically shows the process of strains with different size entering chambers. The budding yeast cells are loaded into microchambers through PDMS degassing and reabsorbing. Medium containing budding yeast cells was indicated with yellow color. For cells of large size strain (average cell diameter larger than 4.2μm which cannot enter the second growth chamber), they were restricted in the first growth chamber (7.1μm-high) and grew in monolayer there after the medium completely entered the last enrichment chamber, and the first growth chamber was chosen to be the observation area. For cells of small size strain (average cell diameter smaller than 4.2μm and larger than 2.0μm), a small part of them may overlapped with each other and thus stayed in the first growth

chamber; but majority of them entered the second growth chamber and were restricted there where they grew in monolayer. In this case, we chose the second growth chamber (4.2μm-high) as the observation area. Supplied with abundant nutrients through diffusion, cells are able to grow exponentially in a monolayer in the restricted microchambers. This design of microfluidic chip ensures that cells are in a single focal plane, enabling high resolution imaging of cell morphology and fluorescent labels over time.

2.2 Budding yeast culture and loading

In the experiments, we prepared the wild type budding yeast and 62 different gene deletion mutant budding yeasts, the details of the name of the gene knocked out can be found in the **Table 1**. In the **Table 1**, we marked the deleted genes with different colors according to gene function. Genes marked with red color are associated with actin cytoskeleton (number 1 to 13); genes marked with green color are associated with cell cycle progression (number 14 to 56); genes marked with blue color are associated with ribosome subunit, ribosome biogenesis and translation (number 57 to 61); gene number 62 relates to vesicle-mediated transport. To mark the cell cycle phase of different strains, an MCM marker fused with an mCherry fluorescent protein was employed in the experiments. When cells are in G_1 phase, the MCM marker is localized in the nucleus and so we can see bright red dots; during non-G_1 phase, the MCM marker is exported from the nucleus and diffused throughout the cytoplasm.[19] The medium for all different strains was synthetic complete medium with Uralic dropped out (SC Ura-). Each colony was picked into a 96 well plate with 0.6mL medium respectively, cultured in a shaker at 30□ overnight (about 15 hours). Then the medium was diluted into fresh medium by a ratio of 1:4, and activated at 30□ for 2 hours. The budding yeast cells are then loaded into microchambers through PDMS degassing and reabsorbing. In the experiments, 2μL medium (OD~0.1) containing different strains was dropped into each well of the chip respectively with multi-channel pipette. After the cells were absorbed into the microchambers, 20μL fresh medium for growth of cells was added to each well with multi-channel pipette. This enables that cells are supplied with abundant nutrients through diffusion so that they

are able to grow exponentially (see supporting information) in a monolayer in the restricted microchambers. Before being mounted on the stage of a microscope, the chip was covered with a 24 mm × 60 mm glass slide which can prevent the evaporation of medium.

2.3 Experimental setup

To monitor the long-time behavior of different strains under same culture condition, we developed the multi-cellular cultivation-observation system. This system consists of two parts: a multi-well timing observations microfluidic chip as the cultivation module; a Nikon Ti inverted microscope equipped with a CCD camera and a programmable motorized stage as the data acquisition module (**Figure 2**a). The multi-well microfluidic chip was mounted on the motorized stage of an inverted microscope, which can perform multi-point data acquisition. The bright field and fluorescence micrographs of different strains in the microfluidic chip were obtained by 40× object lens through *NIS-Elements AR* software. The inverted microscope scanned a series of points of interest (four points for each strain) at a five-minute interval with the help of a motorized stage and a PFS (perfect focus system) focus maintain unit. The prototypical duration of scan is six hours. In the **Figure 2**b, the top panel shows the bright field images of a pair of budding yeast cells; the middle and bottom panels show the corresponding fluorescent images of the same cells. The middle panel shows the micrograph of cells in G_1 phase; the bottom panel shows the cells of non-G_1 phase. It was easy to judge whether cells were in G_1 phase or non-G_1 phase in every fluorescent images using the semi-automatic software. In the experiments, growth chambers where cells were restricted in and grew in monolayer were chosen to be the observation areas, and relative position change of the same cell in any two successive frames was negligible. Therefore, we could trace out the cell moving trajectories as well as the cell lineage relationship, and determined the phase transition time of each cell.

3. Results and discussion

3.1 The method of calculating the doubling time and measuring the cell size for

both mother cells and daughter cells

Figure 3a schematically shows the process of budding yeast cell division. In the experiments, the microscope scanned a series of points of interest at a five-minute interval to obtain both the bright field and fluorescence micrographs of different strains. Here, each black solid arrow represents one interval; each black dotted arrow represents one or more intervals. Cell ① is a mother cell while cell ② is the corresponding daughter cell. We mark the time point when the mother cell ① just enter G_1 phase as $MCTP_1$ (mother cell time point 1) and the time point when the same cell just enter G_1 phase again as $MCTP_2$ (mother cell time point 2), therefore, the mother cell doubling time (MCDT) can be calculated as ($MCTP_2$ - $MCTP_1$). Similarly, we mark the time point when the corresponding daughter cell ② just enter G_1 phase for the first time as $DCTP_1$ (daughter cell time point 1) and the time point when the same cell just enter G_1 phase again as $DCTP_2$ (daughter cell time point 2), so the corresponding daughter cell doubling time (DCDT) can be calculated as ($DCTP_2$ - $DCTP_1$). Meanwhile, we measure the mother cell size (MCS) at the time point $MCTP_1$ and the corresponding daughter cell size (DCS) at the time point $DCTP_1$. Here, $MCTP_2$ and $MCTP_1$, $DCTP_2$ and $DCTP_1$ are all time points, while MCDT and DCDT are both time periods.

In **Figure 3**b, we demonstrate measure example of mother cell size (MCS) at the time point $MCTP_1$ and the corresponding daughter cell size (DCS) at the time point $DCTP_1$. Size measure was carried out in the bright field micrographs through ImageJ, an image processing program. We used two-dimensional cross-sectional area to estimate the size of the mother cell and the corresponding daughter cell. The top and middle panels show the measure of mother cell size and the corresponding daughter cell size, respectively. The two bright field micrographs in the two panels are exactly the same. The bottom panel shows corresponding fluorescence micrograph of the bright field micrographs above. **Figure 3**c shows measure example of mother cell doubling time (MCDT) and the corresponding daughter cell doubling time (DCDT). The cell pointed by the yellow solid arrow is the same mother cell at different time points; another cell pointed by the green solid arrow is the corresponding same daughter cell at different time points. From the timing diagrams of cell division, we

can obtain that $MCTP_1$ = 50 min, $MCTP_2$ = 110 min; $DCTP_1$ = 50 min, $DCTP_2$ = 130 min. Therefore, the conclusion is that MCDT = 60 min and DCDT = 80 min. We also confirmed that the cell doubling time of wild type in our chip is comparable with that in other setup.[4]

3.2 Typical cell morphology comparison of different strains

Phenotypic characteristics of mutants usually provide some clues of gene functions. In our system, besides the cell cycle length and cell size, cell morphology could be easily observed and compared between different strains. **Figure 3**d shows the comparison of cell morphology of several strains. To begin with, a parameter called circularity parameter had been defined as $CP = (4\pi A/P^2)$ where A is the area of the observed cell, and P is the perimeter of the cell.[20] The shape of WT cell is near a normal oval of which the circularity parameter is closed to 1. In contrast to the WT cells (CP=0.97), some mutant cells are similar to the WT cells both in cell size and cell shape. However, some mutant cells showed a different size and their shape somewhat looked like a oval whose circularity parameter was close to that of WT cells, such as *vta1Δ* mutant cells (MCS=1.17; DCS=1.18. CP=0.93), *ctf4Δ* mutant cells (MCS=1.26; DCS=1.37. CP=0.93) and *loc1Δ* mutant cells (MCS=0.92; DCS=0.79. CP=0.96). In addition, some of the cells of other mutants changed a lot both in size and shape, whose shape became very strange and circularity parameter was further smaller than 1. For example, *spc72Δ* (MCS=1.82; DCS=2.07. CP=0.85), *arp5Δ* (MCS=1.44; DCS=1.32. CP=0.79) and *alf1Δ* (MCS=1.47; DCS=1.49. CP= 0.74) strains showed that some cells are relatively large in size; and some of *arp5Δ* and *alf1Δ* cells appeared to be rod-shaped with elongated bud. All of these strange-shaped cells are larger than the WT cells in size on average. Besides, some of mutant cells were fragile and easy to die such as *cap2Δ* mutant cells.

3.3 Statistical results of MCDT, DCDT, MCS and DCS of different strains

Table 1 shows the statistical results of MCDT, DCDT, MCS and DCS of different strains. In the experiments, we prepared the wild-type and 62 single gene deletion strains of the budding yeasts *Saccharomyces cerevisiae*. For each strain, about ten measurements were performed for each parameter (MCDT, DCDT, MCS and DCS) and the average results were calculated. During the about ten measurements, we had confirmed that MCDT/DCDT, MCS/DCS was basically the same with continuous cell

division for all of the strains (see supporting information). The four parameters of all 62 single gene deletion mutants were then normalized relative to the corresponding parameters of the wild type strains. The four average parameters of wild type are: MCDT=80 min and DCDT=95 min, MCS=31.6 μm^2 and DCS=25.2μm^2, we can convert the normalized statistical result to original result by multiply by the corresponding parameters of the wild type. For the majority of the strains, mother cell size is bigger than daughter cell size and mother cell doubling time is shorter than daughter cell doubling time. We have known that cytokinesis is asymmetric regarding cell mass for budding yeast, resulting in a large mother cell and a smaller daughter cell. Hartwell et al. demonstrated that coordination between cell growth and the cell cycle is at the G1/S-phase boundary called Start point. It is a requirement that cells must reach a critical cell size in order to pass the Start point, such that larger mother cell passes through a minor G1 phase while the smaller daughter cell need a long time in G1 phase to attain the critical cell size.[21] Therefore, the asymmetric Cytokinesis and the distinct length of G1 phase can largely account for the differences between mother and daughter cells in their doubling time and cell size. Among the 62 single gene deletion strains, 51 strains present larger cell size and 9 strains present smaller cell size relative to the wild type, 2 mutants have no data (No cell survived in the agar plate).

The 51 single gene deletion strains with large cell size mainly disrupt the genes which either promote the cell cycle progression or execute different cell division events. Generally, genes promoting cell cycle progression are mostly involved in cyclins such as CLN3 and BCK2, transcription factors such as SWI4 and SWI6, and subunit of Anaphase-Promoting Complex/Cyclosome, CDC26. Deletion of these genes delays the progression of cell cycle, leading cells to increase in size.[17] In *bck2Δ* and *cln3Δ* mutant cells, the expression of the G1 phase cyclins CLN1 and CLN2 is delayed, resulting in abnormally large cells (*bck2Δ* (MCS=1.27; DCS=1.17); *cln3Δ* (MCS=1.22; DCS=1.32)). Similarly, for mutant cells lacking two transcription factors, SWI6 or SWI4, the normal expression patterns of CLN1 and CLN2 is disturbed, leading to large cells (*swi6Δ* (MCS=1.20; DCS=1.15); *swi4Δ* (MCS=1.30;

DCS=1.22)) with altered growth rates.[22-25] It has also been demonstrated that these four mutants, *whi2Δ*, *whi3Δ*, *bck2Δ*, and *cln3Δ*, present abnormally cell sizes.[22, 26-27] Besides, CDC26 is also related with promoting cell cycle progression. It is required for degradation of anaphase inhibitors during the metaphase/anaphase transition. For most of CDC mutants, cell division is restricted while cell growth is not affected, which leads to abnormally large cells (*cdc26Δ* (MCS=1.01; DCS=1.11); *cdc50Δ* (MCS=1.05; DCS=1.21).

In addition, genes associated with executing different cell division events are mostly involved in chromosome segregation such as CTF4 and SPC72, spindle pole body separation such as CIN8 and cell separation such as HOF1. The first mutant, *ctf4Δ*, experiences a marked G2/M accumulation of large budded cells and shows defects in S phase entry and S phase progression,[28-29] resulting in abnormally large cell size (MCS=1.26; DCS=1.37). For *cin8Δ* strain, it shows a dramatic delay in the initiation of anaphase and spindles of *cin8Δ* cells elongate slowly during anaphase.[30] Thus, the delayed cell cycle progression in anaphase (Corresponding MCDT=1.84; DCDT=2.29) leads to abnormally large cell size of *cin8Δ* mutant cells (MCS=1.99; DCS=2.47). For another mutant, *hof1Δ*, cells are delayed before cell separation probably because of the defect in the maturation of the septum or in cell separation,[31] leading to large cell size (MCS=2.24; DCS=1.99). The two mutants mentioned above, *cin8Δ* and *hof1Δ*, almost have the largest cell size (MCS~2.00; DCS~2.00) among the 62 mutants.

Meanwhile, the genes whose deletion result in small cell size (9 mutants) generally function to inhibit cell cycle progression. These genes are mainly involved in cell cycle inhibitor such as SWE1 or ribosomal protein such as LOC1 and SCH9. Deletion of these genes generally accelerates the progression of cell cycle, leading mutant cells to decrease in size.[17] In *swe1Δ* mutant cells, cell cycle progression through the G2/M phase transition was increased.[32] Thus, *swe1Δ* mutant cells show short cell cycle (MCDT=0.72; DCDT=0.67) as well as decreased cell size (MCS=0.90; DCS=0.83) relative to WT. In another mutant, *loc1Δ*, cells are severely impaired for growth,[33] resulting in abnormally small cell size (MCS=0.92; DCS=0.79). The two mutants

mentioned above, *swe1Δ* and *loc1Δ*, almost have the abnormally smallest cell size (MCS~0.90; DCS~0.90) among the 62 mutants.

Deletion of genes involved in cytoskeleton also shows distinct cell size in our data mainly because of the change of the cell shape. We notice that among all the 62 mutant strains most cells of three strains (*spc72Δ*, *arp5Δ*, *alf1Δ*) mentioned previously in **Figure 3**d have irregular shape. Among the 3 genes, SPC72 has roles in astral microtubule formation and stabilization, ARP5 is one of actin-related proteins which can assist dynein in catalyzing microtubule-based motility,[34] and ALF1 gene displays genetic interactions with the tubulin genes and other genes involved in microtubule function.[35] The three mutants all showed elongated bud,[36] strange cell shape and abnormally large cell size (*spc72Δ* (MCS=1.82; DCS=2.07), *arp5Δ* (MCS=1.44; DCS=1.32) and *alf1Δ* (MCS=1.47; DCS=1.49)) which may result from the defective of the cytoplasmic microtubules.[37]

As we analyzed above, most deletion of genes which affect the cell cycle length alters the cell size, but actually our data also show that not all the longer cell cycle result in larger cells or shorter cell cycle lead to smaller ones. The reason maybe that the separate phase (G1, S and M phase) is only part of the whole cell cycle. Delay in one phase of the whole cell cycle didn't necessarily result in longer cell cycle. In addition, cell cycle is also related to cell growth.[38] Besides, some other strains shown larger cell size is due to the deletion of gene involved in cytoskeleton (*spc72Δ*, *arp5Δ*, *alf1Δ*), not because of change in cell cycle. That is to say, there is no necessary correlation between the cell size and the length of cell cycle, which also has been demonstrated by previous study with flow cytometry.[18] We consider the reason may be that the perturbation also changes the cell growth rate, which is coordinated with cell cycle to reach size homeostasis.[38] In our system, we could not only extract the cell cycle length but also the cell growth rate. In future, it would be useful to considering these two parameters together to understand how the cell achieve the size homeostasis in constant environment by coordinating cell growth and cell division.

4. Conclusion

In this paper, we presented a novel, facile and robust multi-well microfluidic system for high-throughput tracking of different budding yeast strains in single-cell level. We can high-throughput load different strains into this system and provide monolayer growth conditions for the strains. This system could allow us to get multi-dimension parameters (such as cell size, doubling time and protein expression level) of 32 strains in parallel in one single experiment from the time-lapse movie. In the experiment, wild type and 62 single gene deletion strains were chosen for scanning as a demonstration. We measured the doubling time and cell size for mother cell and daughter cell, respectively. Meanwhile, we compared typical cell morphology of different strains and analyzed the relationship between cell genotype and phenotype.

In the future, this new system can be used not only for analysis of the doubling time and cell size/cell morphology, but also for analysis of protein expression level, protein dynamics, protein localization, cell division and the correlation between them. In addition, it can not only be used for single mutation analysis, but also can be used for the studies of gene-gene interaction. But, this method still has some limitation, one of which is the conflict of time resolution and the number of the sample points being scanned. For five minutes interval, our microscope can scan over 100 sample points and capture one bright field figure and one fluorescence figure for each sample point. More sensitive or large view area CCD may cut down the expose time or sample points for each strain, which may increase the time resolution thus the number of strains being scanned in a single experimental run.

Acknowledgements

We would like to thank X. J. Zhu, G. W. Si, Y. Tian, Y. G. Wang for helpful discussions. This work is partially supported by the NSF of China (10721403, 11074009, 11174012), the MOST of China (2009CB918500, 2012AA02A702), the NFFTBS of China (J0630311).

References

1. P. G. Lord and A. E. Wheals, Variability in individual cell cycles of Saccharomyces cerevisiae, *J. Cell Sci.*, 1981, **50**, 361-376.

2 Y. Tian, C. X. Luo, Y. H. Lu, C. Tang and Q. Ouyang, Cell cycle synchronization by nutrient modulation, *Integr. Biol.*, 2012, **4**, 328-334.

3 A. Groisman, C. Lobo, H. J. Cho, J. K. Campbell, Y. S. Dufour, A. M. Stevens and A. Levchenko, A microfluidic chemostat for experiments with bacterial and yeast cells, *Nat. Methods*, 2005, **2**, 685-689.

4 C. X. Luo, L. L. Jiang, S. B. Liang, Q. Ouyang, H. Ji and Y. Chen, High-throughput microfluidic system for monitoring diffusion-based monolayer yeast cell culture over long time periods, *Biomed. Microdevices*, 2009, **11**, 981-986.

5 F. K. Balagadde, L. C. You, C. L. Hansen, F. H. Arnold and S. R. Quake, Long-term monitoring of bacteria undergoing programmed population control in a microchemostat, *Science*, 2005, **309**, 137-140.

6 G. Charvin, F. R. Cross and E. D. Siggia, A Microfluidic Device for Temporally Controlled Gene Expression and Long-Term Fluorescent Imaging in Unperturbed Dividing Yeast Cells, *Plos One*, 2008, **3**.

7 D. Falconnet, A. Niemisto, R. J. Taylor, M. Ricicova, T. Galitski, I. Shmulevich and C. L. Hansen, High-throughput tracking of single yeast cells in a microfluidic imaging matrix, *Lab Chip*, 2011, **11**, 466-473.

8 A. C. Rowat, J. C. Bird, J. J. Agresti, O. J. Rando and D. A. Weitz, Tracking lineages of single cells in lines using a microfluidic device, *Proc. Natl. Acad. Sci. U. S. A.*, 2009, **106**, 18149-18154.

9 M. Ricicova, M. Hamidi, A. Quiring, A. Niemisto, E. Emberly and C. L. Hansen, Dissecting genealogy and cell cycle as sources of cell-to-cell variability in MAPK signaling using high-throughput lineage tracking, *Proc. Natl. Acad. Sci. U. S. A.*, 2013, **110**, 11403-11408.

10 G. Sorg, H. D. Schubert, F. H. Buttner and R. Heilker, Automated high throughput screening for serine kinase inhibitors using a LEADSeeker (TM) scintillation proximity assay in the 1536-well format, *J. Biomol. Screen.*, 2002, **7**, 11-19.

11 R. P. Hertzberg and A. J. Pope, High-throughput screening: new technology for the 21st century, *Curr. Opin. Chem. Biol.*, 2000, **4**, 445-451.

12 M. F. Zettel, L. R. Garza, A. M. Cass, R. A. Myhre, L. A. Haizlip, S. N.

Osadebe, D. W. Sudimack, R. Pathak, T. L. Stone and M. Polymenis, The budding index of Saccharomyces cerevisiae deletion strains identifies genes important for cell cycle progression, *Fems Microbiol. Lett.*, 2003, **223**, 253-258.

13 J. P. Nolan and L. A. Sklar, The emergence of flow cytometry for sensitive, real-time measurements of molecular interactions, *Nat. Biotechnol.*, 1998, **16**, 633-638.

14 W. K. Huh, J. V. Falvo, L. C. Gerke, A. S. Carroll, R. W. Howson, J. S. Weissman and E. K. O'Shea, Global analysis of protein localization in budding yeast, *Nature*, 2003, **425**, 686-691.

15 C. Hansen and S. R. Quake, Microfluidics in structural biology: smaller, faster... better, *Curr. Opin. Struct. Biol.*, 2003, **13**, 538-544.

16 J. J. Turner, J. C. Ewald and J. M. Skotheim, Cell Size Control in Yeast, *Curr. Biol.*, 2012, **22**, R350-R359.

17 P. Jorgensen, J. L. Nishikawa, B. J. Breitkreutz and M. Tyers, Systematic identification of pathways that couple cell growth and division in yeast, *Science*, 2002, **297**, 395-400.

18 S. A. Hoose, J. A. Rawlings, M. M. Kelly, M. C. Leitch, Q. O. Ababneh, J. P. Robles, D. Taylor, E. M. Hoover, B. Hailu, K. A. McEnery, S. S. Downing, D. Kaushal, Y. Chen, A. Rife, K. A. Brahmbhatt, R. Smith and M. Polymenis, A Systematic Analysis of Cell Cycle Regulators in Yeast Reveals That Most Factors Act Independently of Cell Size to Control Initiation of Division, *Plos Genet.*, 2012, **8**.

19 M. E. Liku, V. Q. Nguyen, A. W. Rosales, K. Irie and J. J. Li, CDK phosphorylation of a novel NLS-NES module distributed between two subunits of the Mcm2-7 complex prevents chromosomal rereplication, *Mol. Biol. Cell*, 2005, **16**, 5026-5039.

20 D. R. Gossett, H. T. K. Tse, S. A. Lee, Y. Ying, A. G. Lindgren, O. O. Yang, J. Y. Rao, A. T. Clark and D. Di Carlo, Hydrodynamic stretching of single cells for large population mechanical phenotyping, *Proc. Natl. Acad. Sci. U. S. A.*, 2012, **109**, 7630-7635.

21 G. C. Johnston, J. R. Pringle and L. H. Hartwell, Coordination of growth with cell division in the yeast Saccharomyces cerevisiae, *Exp. Cell Res.*, 1977, **105**, 79-98.

22 P. E. Sudbery, A. R. Goodey and B. L. A. Carter, Genes which control cell proliferation in the yeast Saccharomyces cerevisiae, *Nature*, 1980, **288**, 401-404.

23 P. Radcliffe, J. Trevethick, M. Tyers and P. Sudbery, Deregulation of CLN1 and CLN2 in the Saccharomyces cerevisiae whi2 mutant, *Yeast*, 1997, **13**, 707-715.

24 R. S. Nash, T. Volpe and B. Futcher, Isolation and characterization of WHI3, a size-control gene of Saccharomyces cerevisiae, *Genetics*, 2001, **157**, 1469-1480.

25. J. Zhang, C. Schneider, L. Ottmers, R. Rodriguez, A. Day, J. Markwardt and B. L. Schneider, Genomic scale mutant hunt identifies cell size homeostasis genes in S-cerevisiae, *Curr. Biol.*, 2002, **12**, 1992-2001.

26 C. J. Dicomo, H. Chang and K. T. Arndt, Activation of CLN1 and CLN2 G1 cyclin gene expression by BCK2, *Mol. Cell. Biol.*, 1995, **15**, 1835-1846.

27 L. Dirick, T. Bohm and K. Nasmyth, Roles and regulation of Cln-Cdc28 kinases at the start of the cell cycle of Saccharomyces cerevisiae, *Embo J.*, 1995, **14**, 4803-4813.

28 N. Kouprina, E. Kroll, V. Bannikov, V. Bliskovsky, R. Gizatullin, A. Kirillov, V. Zakharyev, P. Hieter, F. Spencer and V. Larionov, CTF4 (CHL15) mutants exhibit defective DNA metabolism in the yeast Saccharomyces cerevisiae, *Mol. Cell. Biol.*, 1992, **12**, 5736-5747.

29 J. Wang, R. Wu, Y. Lu and C. Liang, Ctf4p facilitates Mcm10p to promote DNA replication in budding yeast, *Biochem. Biophys. Res. Commun.*, 2010, **395**, 336-341.

30 A. F. Straight, J. W. Sedat and A. W. Murray, Time-lapse microscopy reveals unique roles for kinesins during anaphase in budding yeast, *J. Cell Biol.*, 1998, **143**, 687-694.

31 E. A. Vallen, J. Caviston and E. Bi, Roles of Hof1p, Bni1p, Bnr1p, and Myo1p

in cytokinesis in Saccharomyces cerevisiae, *Mol. Biol. Cell*, 2000, **11**, 593-611.

32 T. Shiga, H. Suzuki, A. Yamamoto, H. Yamamoto and K. Yamamoto, Hydroquinone, a Benzene Metabolite, Induces Hog1-dependent Stress Response Signaling and Causes Aneuploidy in Saccharomyces cerevisiae, *J. Radiat. Res.*, 2010, **51**, 405-415.

33 C. R. Urbinati, G. B. Gonsalvez, J. P. Aris and R. M. Long, Loc1p is required for efficient assembly and nuclear export of the 60S ribosomal subunit, *Mol. Genet. Genomics*, 2006, **276**, 369-377.

34 D. A. Schafer and T. A. Schroer, Actin-related proteins, *Annu. Rev. Cell Dev. Biol.*, 1999, **15**, 341-363.

35 B. Feierbach, E. Nogales, K. H. Downing and T. Stearns, Alf1p, a CLIP-170 domain-containing protein, is functionally and physically associated with alpha-tubulin, *J. Cell Biol.*, 1999, **144**, 113-124.

36 M. Watanabe, D. Watanabe, S. Nogami, S. Morishita and Y. Ohya, Comprehensive and quantitative analysis of yeast deletion mutants defective in apical and isotropic bud growth, *Curr. Genet.*, 2009, **55**, 365-380.

37 H. Maekawa, C. Priest, J. Lechner, G. Pereira and E. Schiebel, The yeast centrosome translates the positional information of the anaphase spindle into a cell cycle signal, *J. Cell Biol.*, 2007, **179**, 423-436.

38 M. M. Swann, The Control of Cell Division: A Review 1. General Mechanisms, *Cancer Res.*, 1957, **17**, 727-757.

Figure captions

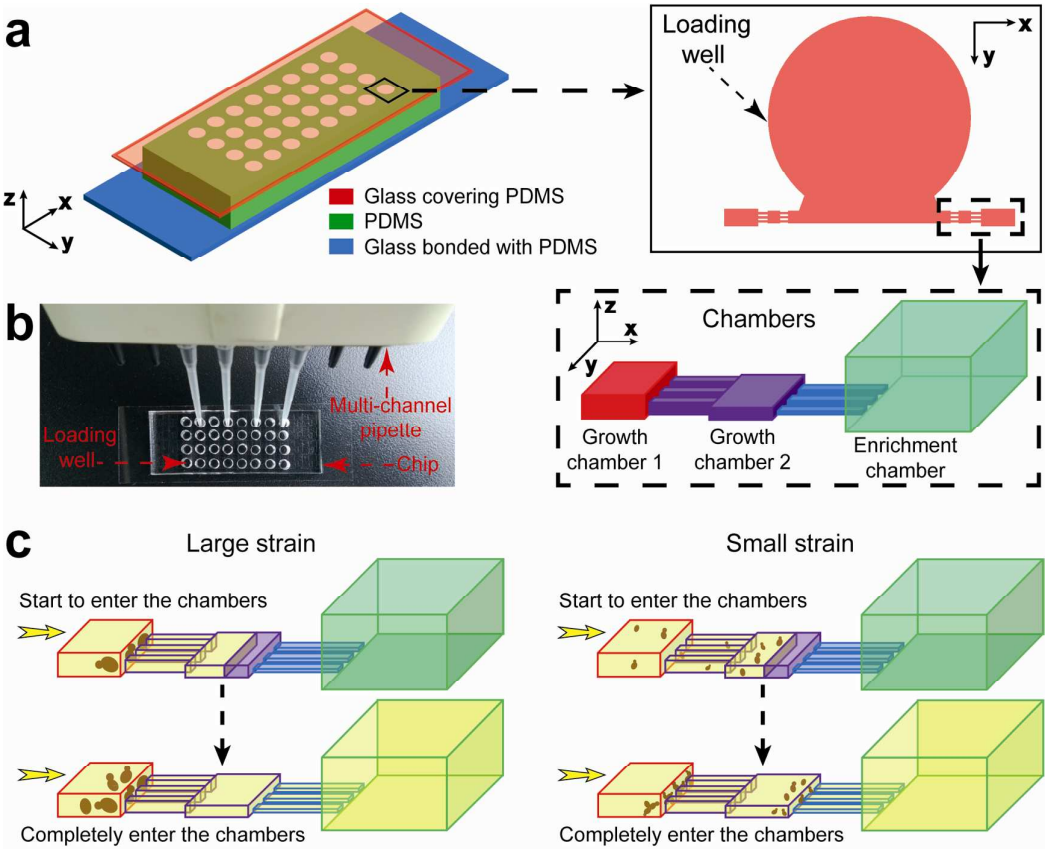

Figure 1. a) A schematic image of our microfluidic chip design (not to scale). **b)** Photo of the microfluidic chip which is under operation. Different budding yeast samples were dropped into each well through multi-channel pipette. **c)** Schematic images of process of strains of different size entering restricted chambers.

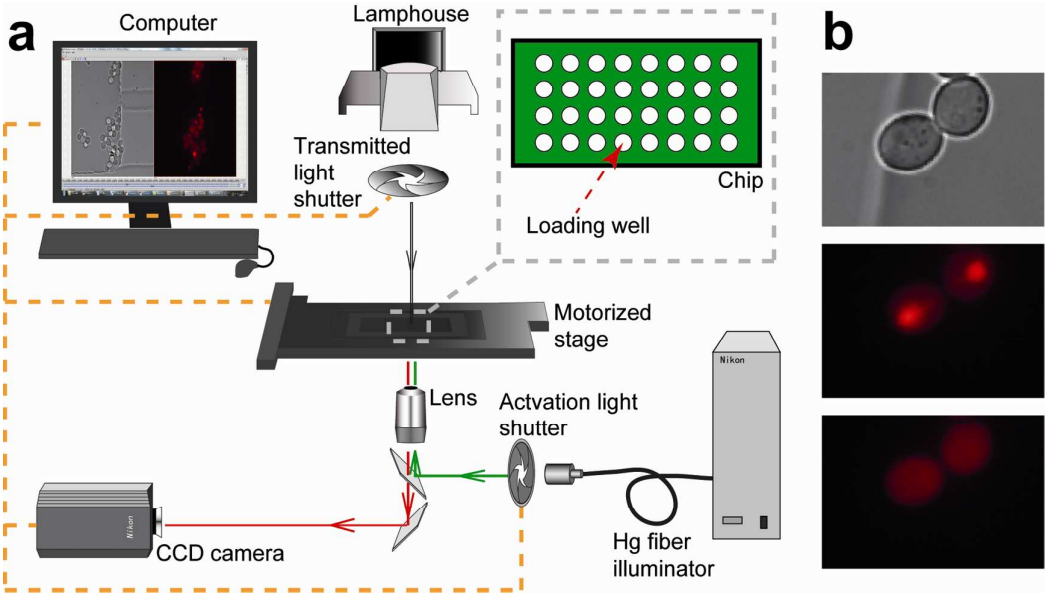

Figure 2. Microfluidic system used in the experiments. **a)** The multi-well microfluidic chip was mounted on the motorized stage of an inverted microscope, which can perform multi-point data acquisition. Both fluorescent and bright field images of cells could be acquired by the CCD camera, which were shown in the screen of computer. The inset shows the layout of our microfluidic chip. **b)** The top panel shows the bright field images of a pair of budding yeast cells; the middle and bottom panels show the corresponding fluorescent images of the same cells. The middle panel shows the micrograph of cells in G_1 phase, in which the MCM marker is localized in the nucleus and so we can see bright red dots; the bottom panel shows the cells of non-G_1 phase in which the MCM marker is diffused throughout the cytoplasm.

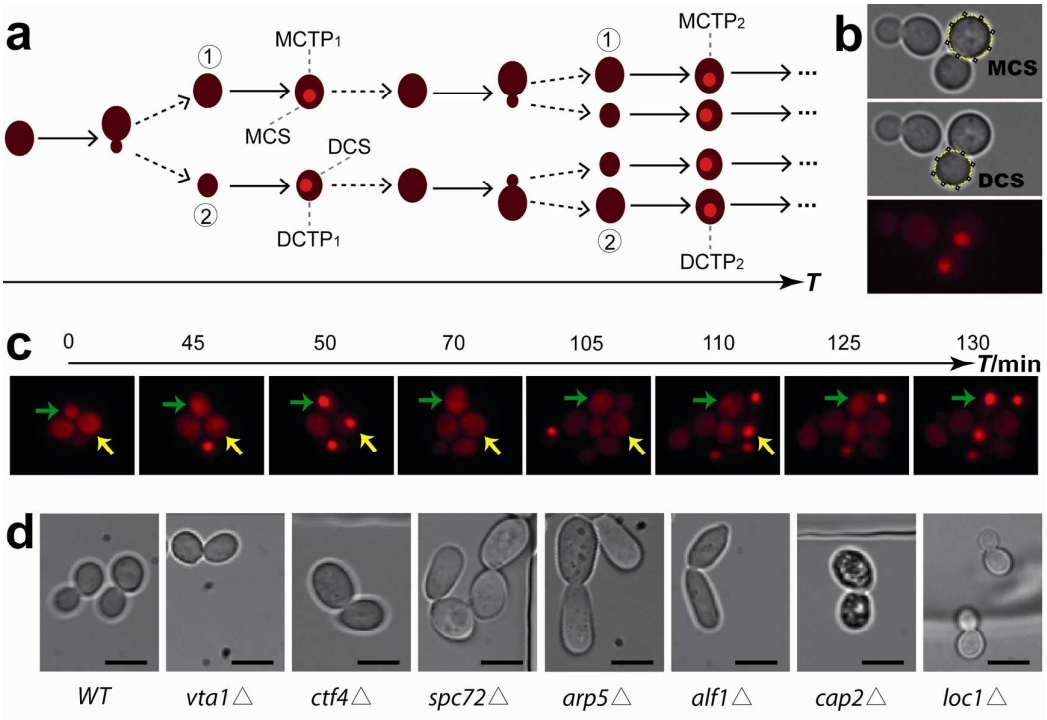

Figure 3. a) Schematic fluorescence diagrams of the process of budding yeast cell division. **b)** Measurement example of mother cell size (MCS) at the time point $MCTP_1$ and the corresponding daughter cell size (DCS) at the time point $DCTP_1$. **c)** Measurement example of mother cell doubling time (MCDT) and the corresponding daughter cell doubling time (DCDT). **d)** Comparison of typical cell morphology of several strains (scale bar 10 μm).

No.	Deleted gene	MCDT	DCDT	MCS	DCS	Function
00#	WT	1	1	1	1	
01#	FIG4	0.76±0.09	0.77±0.06	0.97±0.17	0.92±0.11	Actin cytoskeleton
02#	CLA4	0.91±0.10	0.86±0.09	0.93±0.15	1.00±0.23	Actin cytoskeleton
03#	MDM20	1.14±0.11	1.19±0.04	1.13±0.17	1.09±0.16	Actin cytoskeleton
04#	BEM4	1.28±0.22	1.21±0.33	1.09±0.16(1.29)	1.15±0.20(1.13)	Actin cytoskeleton
05#	BEM1	0.82±0.09	0.79±0.08	1.16±0.21(1.59)	1.09±0.22(1.35)	Actin cytoskeleton
06#	RVS161	0.81±0.12	0.73±0.05	1.16±0.18(1.34)	1.12±0.25(1.35)	Actin cytoskeleton
07#	SAC3	0.89±0.07	1.14±0.17	1.06±0.14(1.32)	1.09±0.17(1.22)	Actin cytoskeleton
08#	CAP2†	1.00±0.06	0.75±0.11	1.50±0.31(1.15)	1.40±0.14(1.13)	Actin cytoskeleton
09#	RHO4	0.83±0.12	0.70±0.15	1.12±0.16(1.39)	1.10±0.15(1.26)	Actin cytoskeleton
10#	VRP1	1.12±0.09	0.83±0.20	1.16±0.22(1.17)	1.22±0.34(?)	Actin cytoskeleton
11#	ARP5*	1.17±0.06	1.09±0.11	1.44±0.26(1.66)	1.32±0.20(?)	Actin cytoskeleton
12#	BEM2	1.01±0.18	0.87±0.20	1.15±0.31(1.10)	1.16±0.37(?)	Actin cytoskeleton
13#	MRC1	1.07±0.21	1.02±0.32	1.17±0.39(1.54)	1.02±0.24(1.17)	Actin cytoskeleton
14#	CLN3	0.85±0.16	0.93±0.15	1.22±0.26(1.44)	1.32±0.25(?)	Cell cycle
15#	YKU70	0.83±0.06	0.77±0.08	1.02±0.08	0.95±0.18	Cell cycle
16#	RTS1	0.88±0.07	1.01±0.20	1.30±0.15(1.34)	1.36±0.18(1.52)	Cell cycle
17#	DIA2	1.03±0.14	0.96±0.14	0.91±0.13	1.01±0.16	Cell cycle
18#	WHI5	1.03±0.10	1.07±0.25	1.07±0.19	1.24±0.28	Cell cycle
19#	CDC40†	–	–	–	–	Cell cycle
20#	CIN8	1.84±0.63	2.29±0.09	1.99±0.25(1.71)	2.47±0.19(1.70)	Cell cycle
21#	DCC1	1.43±0.35	1.45±0.19	1.10±0.06(1.34)	1.29±0.18(1.30)	Cell cycle
22#	ACE2	0.74±0.16	0.86±0.08	1.39±0.38(1.44)	1.31±0.16(?)	Cell cycle
23#	CDC10	0.99±0.18	1.17±0.23	1.60±0.26(1.71)	1.84±0.43(1.78)	Cell cycle
24#	VTA1	1.09±0.11	0.86±0.14	1.17±0.18	1.18±0.15	Cell cycle
25#	HSL1	1.18±0.26	0.96±0.17	1.17±0.14(1.27)	1.34±0.25(1.30)	Cell cycle
26#	PAC10†	–	–	–	–	Cell cycle
27#	SWI6	0.89±0.10	0.92±0.09	1.20±0.20(1.41)	1.15±0.20(1.30)	Cell cycle
28#	SWE1	0.72±0.03	0.67±0.08	0.90±0.09(0.90)	0.83±0.10(0.78)	Cell cycle
29#	EST1	1.11±0.04	1.30±0.15	1.26±0.24(1.12)	1.41±0.31(1.00)	Cell cycle
30#	EST2	0.87±0.05	0.86±0.12	1.11±0.18(1.29)	1.13±0.22(?)	Cell cycle
31#	YKE2	1.26±0.13	1.50±0.17	1.30±0.44(1.32)	1.35±0.37(?)	Cell cycle
32#	CDH1	0.93±0.18	1.15±0.19	1.47±0.46	1.55±0.39	Cell cycle
33#	WHI3	0.91±0.17	0.76±0.14	1.03±0.20(1.10)	0.97±0.13(0.74)	Cell cycle
34#	CDC50	0.94±0.18	1.15±0.20	1.05±0.26(1.20)	1.21±0.32(1.30)	Cell cycle
35#	CDC26	0.97±0.00	0.97±0.00	1.01±0.20(1.20)	1.11±0.17(1.17)	Cell cycle
36#	CLB2	1.12±0.15	1.23±0.30	1.17±0.18(1.51)	1.34±0.11(1.65)	Cell cycle
37#	CTF4	1.00±0.13	0.92±0.11	1.26±0.28	1.37±0.30	Cell cycle
38#	PIN4	1.30±0.37	0.86±0.18	1.17±0.28	1.24±0.34	Cell cycle
39#	ALF1*	1.07±0.07	1.08±0.27	1.47±0.20(1.44)	1.49±0.21(1.39)	Cell cycle
40#	GIM5	1.16±0.21	0.85±0.07	1.16±0.26(1.10)	1.08±0.31(1.09)	Cell cycle
41#	RAD50	1.37±0.16	0.93±0.25	1.44±0.41(1.27)	1.22±0.27(1.13)	Cell cycle
42#	RAD5	1.01±0.25	1.30±0.49	1.20±0.20(1.27)	1.23±0.25(1.04)	Cell cycle
43#	PAP2	0.90±0.08	0.72±0.08	1.20±0.12	1.26±0.14	Cell cycle
44#	DPB3	1.19±0.22	1.22±0.28	1.12±0.10(1.02)	1.21±0.15(1.65)	Cell cycle
45#	SPC72*	1.32±0.16	0.87±0.07	1.82±0.28(1.59)	2.07±0.22(?)	Cell cycle
46#	DBF2	1.23±0.13	0.84±0.00	1.20±0.16(1.27)	1.15±0.20(1.43)	Cell cycle
47#	CIK1	1.17±0.04	0.76±0.11	1.46±0.48(1.46)	1.42±0.53(1.48)	Cell cycle
48#	BRE1	1.40±0.46	0.83±0.06	1.28±0.54(1.22)	1.17±0.51(1.26)	Cell cycle
49#	BCK2	1.09±0.25	1.22±0.11	1.27±0.22(1.39)	1.17±0.20(1.22)	Cell cycle
50#	SWI4	1.01±0.06	0.83±0.06	1.30±0.29(1.71)	1.22±0.24(1.91)	Cell cycle
51#	TPD3	1.12±0.06	1.20±0.34	0.93±0.16(0.80)	0.90±0.22(?)	Cell cycle
52#	RNR1	0.92±0.09	1.04±0.04	1.54±0.32(2.05)	1.57±0.34(2.26)	Cell cycle
53#	BUB3	1.46±0.41	1.36±0.27	1.49±0.32(1.29)	1.62±0.32(1.04)	Cell cycle
54#	KAR3	1.00±0.14	0.84±0.09	1.11±0.20(1.34)	1.10±0.22(?)	Cell cycle
55#	RNR4	1.33±0.16	1.26±0.19	1.71±0.64(1.66)	1.53±0.38(1.61)	Cell cycle
56#	HOF1	0.96±0.18	1.04±0.33	2.24±0.84(1.78)	1.99±0.83(?)	Cell cycle
57#	BUD20	0.99±0.24	0.88±0.06	1.07±0.17	1.06±0.16	Ribosome, translation
58#	LOC1	2.09±0.00	2.37±0.00	0.92±0.13(0.85)	0.79±0.04(0.65)	Ribosome, translation
59#	CTK2†	1.09±0.50	1.05±0.43	0.99±0.15	1.02±0.17	Ribosome, translation
60#	SFP1	1.40±0.26	1.33±0.28	1.00±0.28	1.01±0.25	Ribosome, translation
61#	SCH9	1.39±0.19	1.39±0.19	0.94±0.25(0.67)	0.87±0.22(0.39)	Ribosome, translation
62#	CLC1	0.95±0.12	0.97±0.27	0.99±0.12	0.98±0.18	Vesicle-mediated transport

†: Cells were fragile and were easy to die *: Shape of most cells was irregular

Table 1. Statistical results of MCDT, DCDT, MCS and DCS of different strains. In the experiments, we prepared the wild-type and 62 single gene deletion mutant strains of the budding yeasts *Saccharomyces cerevisiae*. The four parameters (MCDT, DCDT, MCS and DCS) of all 62 single gene deletion mutant cells were normalized relative to the corresponding parameters of the wild type cells. The data (?: No data available) in parentheses are statistical results quoted from studies of Jorgensen et al. that utilized Beckman-Coulter.[17] *: Shape of most cells was irregular; †: Cells were fragile and were easy to die (No cell survived in the agar plate for some mutants (—: No data); some mutant cells stopped dividing or died during imaging processes).